MECSOL 2022 - Proceedings of the 8th International Symposium on Solid Mechanics
M.L. Bittencourt, J. Labaki, L.C.M. Vieira Jr. and E. Mesquita (Editors), Campinas SP, Brazil, October 17th to 19th, 2022

On the use of recovered stresses to improve the accuracy of the contour integral method in the computation of stress intensity factors

Rafael Lins [1], Mariano Arbelo [1], Francisco Alex Monteiro [1] and Sérgio Cordeiro [1]

[1] Aeronautics Institute of Technology (ITA), Praça Marechal Eduardo Gomes, 50, Vila das Acácias, 12228-900, São José dos Campos/SP - Brazil

Abstract: This work aims to assess the effect of the replacement of the raw stresses by the recovered stresses on the computation of stress intensity factors (SIFs) using the contour integral method (CIM). The raw stresses are computed by means of two distinct methodologies: the generalized finite element method (GFEM) and the stable generalized finite element method (SGFEM). For both methods, the adopted enrichment functions aim to emulate the discontinuities introduced by the crack and also to represent the singularity effects nearby to the crack tip. Furthermore, in the SGFEM, these enrichment functions are slightly modified to overcome some drawbacks commonly associated to GFEM, like decrease of convergence rate due to ill conditioning of the stiffness matrix. The recovered stresses, in turn, are obtained using a procedure based on a locally weighted L^2 projection, which leads to a very computationally efficient block-diagonal system of equations. In the open literature, the recovered stresses are usually computed from the minimization of an error functional and by consequence these stresses, in general, are more accurate than the raw stresses. Such feature is often explored to build error estimators, however in this work a novel application for the recovered stresses is presented, once now they are implemented aiming to improve the accuracy of a SIF extraction method. The CIM was chosen as extraction method due to the following features: it presents a high accuracy comparable to J integral and its numerical implementation is less complex than the cutoff function method (CFM). Finally, numerical examples are presented to demonstrate the benefits associated to application of the recovered stresses using both GFEM and SGFEM methodologies. These examples address different opening modes as well as horizontal and inclined cracks. Aspects as accuracy and path independent property are discussed.

Keywords: stress intensity factor, generalized finite element method, contour integral method, recovered stresses

INTRODUCTION

Stress intensity factors (SIFs) are one of the most important parameters in fracture mechanics: they define the amplitude of the crack-tip singularity (Anderson, 2005). Such parameters also allow to assess: (i) if a crack will propagate or not and (ii) the crack propagation direction. There are several different extraction methods for the SIFs. The most accurate methods are those based on energy release rate, as for instance: the J integral (Rice, 1968), the Interaction Integrals (Yau et al., 1980), the Cutoff Function Method (CFM) (Szabó and Babuŝka, 1991) and the Contour Integral Method (CIM) (Szabó and Babuŝka, 1991). In general, these methods present high accuracy and theoretically independency of the path used to calculate the SIFs. However, such features are directly associated with the quality of the solution discretization method.

The improvement of the stress field accuracy is one of main features of the Generalized Finite Element Method (GFEM) (Duarte et al., 2000; Belytschko et al. 2009). In this method, the approximation solution space is augmented by using enrichment functions, reducing thus excessive mesh refinements and allowing accurate results near crack tips without the inconvenient of adjusting the mesh at the crack faces. However, the enrichment function set can introduce linear dependencies, that will provide ill-conditioning to the problem solver. Babuŝka and Banerjee (2012) proposed a modification in the GFEM formulation, entitled as Stable Generalized Finite Element Method (SGFEM), that overcome this drawback.

Formulations based on displacement field as the FEM or the GFEM naturally present stress fields less accurate than displacement fields, since the stress, by definition, is related to the derivative of the displacements. Consequently, much research has been developed to improve the stress accuracy. One idea to do this consists on employing the same shape functions used in displacement interpolation to define new stress fields based on nodal stress values, computed by means of the minimization of a functional in a least squares sense. This idea was originally presented in Zienkiewicz and Zhu (1987). The improved new stress field is known as recovered stress field and can be utilized to build an error estimator. The Zienkiewicz and Zhu ideas were extended for the eXtended Finite Element Method (XFEM) in Prange et

al. (2012) and for the SGFEM in Lins et al. (2015). Lins et al. (2019) presented a new version of the recovery procedure introduced in Lins et al. (2015). Now a block-diagonal system of equations is responsible to calculate the recovered stresses. Such change, in general, preserved the accuracy and improved the computational efficiency.

This work aims to describe a novel application for the recovered stresses previously described, in which they are now being used to increase the quality of SIFs computed via CIM considering solutions provided by the GFEM and the SGFEM. The CIM was chosen as extraction method due to the following features: it presents a high accuracy comparable to J integral and its numerical implementation is less complex than the CFM (Pereira and Duarte, 2005). The procedure chosen to calculate the recovered stresses is described in details in Lins et al. (2019). The impact in terms of accuracy and path independence feature due to the replacement of the raw stresses by the recovered stresses are analyzed in two examples. These examples address different opening modes as well as horizontal and inclined cracks.

GFEM AND SGFEM: FORMULATION AND ADOPTED ENRICHMENT FUNCTIONS

Formulation

The GFEM is a numerical method that explores the partition of unity concept to reproduce functions in the approximation that mimic features of sought solution. These functions, known as enrichment functions, enlarge the standard FE approximation shifting the shape functions. The GFEM shape functions, $\phi_{\alpha i}$, attached to the vertex α are commonly given by the product between the Lagrangian shape functions, φ_α, and the enrichment functions, $L_{\alpha i}$. Thus,

$$\phi_{\alpha i} = \varphi_\alpha L_{\alpha i} \left(\text{no summation on } \alpha\right), \tag{1}$$

where α refers to the nodal cloud (set of elements sharing the same node), i (=1,…, nl) identifies the enrichment function, and nl is the total number of enrichment functions applied in each cloud (node).

Restricting to 2D problems, the GFEM approximation for each component of the displacement field is given by

$$\hat{u} = \underbrace{\sum_{\alpha=1}^{n} \varphi_\alpha u_\alpha}_{FEM} + \underbrace{\sum_{\alpha=1}^{n} \varphi_\alpha \left(\sum_{i=2}^{nl} L_{\alpha i} b_{\alpha i} \right)}_{Enrichment} \tag{2}$$

$$\hat{v} = \underbrace{\sum_{\alpha=1}^{n} \varphi_\alpha v_\alpha}_{FEM} + \underbrace{\sum_{\alpha=1}^{n} \varphi_\alpha \left(\sum_{i=2}^{nl} L_{\alpha i} c_{\alpha i} \right)}_{Enrichment}, \tag{3}$$

where n corresponds to total number of nodes, u_α and v_α are parameters associated with usual degrees of freedom of FEs, a $b_{\alpha i}$ and $c_{\alpha i}$ are new degrees of freedom introduced by the enrichment.

As previously mentioned, in the GFEM, any type of function can be used as enrichment and, by consequence, certain functions may affect negatively the conditioning of the stiffness matrix. An ill-conditioned stiffness matrix may lead to results polluted by round-off errors. The SGFEM emerged precisely to overcome such hurdle. The basic difference between the GFEM and the SGFEM from a formulation point of view is a modification of the enrichment functions. In the SGFEM, the enrichment functions are constructed by the difference between the original enrichment function ($L_{\alpha i}$) and its piecewise linear or bilinear finite element interpolant function (I_α). In other words,

$$L_{\alpha i}^{\text{mod}} = L_{\alpha i} - I_\alpha \left(L_{\alpha i}\right) = L_{\alpha i} - \sum_{j=1}^{ne} \varphi_j \left(x, y\right) L_{\alpha i} \left(x_j, y_j\right), \tag{4}$$

where (x_j, y_j) are the coordinates of node j of the element in question and ne refers to the number of element nodes.

The same procedure for constructing the GFEM shape functions is used to define the SGFEM shape functions ($\phi_{\alpha i}^{\text{mod}}$). Hence,

$$\phi_{\alpha i}^{\text{mod}} = \varphi_\alpha L_{\alpha i}^{\text{mod}} \tag{5}$$

More information about the GFEM and the SGFEM formulations can be found in Fries and Belytschko (2010) and Gupta et al. (2013), respectively.

Adopted enrichment functions

Singular enrichments

The following functions introduced in the work of Oden and Duarte (1997) (and hereafter denoted as OD) were chosen as enrichment, aiming to represent the singular behavior near to the crack tip:

$$\begin{aligned} L_{OD-\bar{x}} &= \left\{ \sqrt{r}\left[\left(\kappa-\frac{1}{2}\right)\cos\frac{\theta}{2}-\frac{1}{2}\cos\frac{3\theta}{2}\right], \sqrt{r}\left[\left(\kappa+\frac{3}{2}\right)\sin\frac{\theta}{2}+\frac{1}{2}\sin\frac{3\theta}{2}\right]\right\} \\ L_{OD-\bar{y}} &= \left\{ \sqrt{r}\left[\left(\kappa+\frac{1}{2}\right)\sin\frac{\theta}{2}-\frac{1}{2}\sin\frac{3\theta}{2}\right], \sqrt{r}\left[\left(\kappa-\frac{3}{2}\right)\cos\frac{\theta}{2}+\frac{1}{2}\cos\frac{3\theta}{2}\right]\right\}, \end{aligned} \tag{6}$$

where r and θ are polar coordinates attached to the crack tip, $-\pi < \theta < \pi$, κ is a material constant (3-4ν), and ν is the Poisson ratio. The first set of functions is used for enrichment of the approximation along the local $\bar{x}$ direction and the second is used for enrichment along the local $\bar{y}$ direction.

Discontinuous enrichments

The discontinuity introduced by the presence of the crack is captured by linear Heaviside function given by

$$H_L = \left\{ H, H\frac{(x-x_\alpha)}{h_\alpha}, H\frac{(y-y_\alpha)}{h_\alpha} \right\}, \tag{7}$$

where H represents the standard Heaviside function, i.e:

$$H = \begin{cases} 1 & \text{if } \bar{y} \geq 0 \\ 0 & \text{if } \bar{y} < 0 \end{cases}, \tag{8}$$

and x and y are global coordinates and h_α is a scaling factor given by the diameter of the largest element sharing node α.

THE CONTOUR INTEGRAL METHOD

In this section is presented a summarized version of the formulation of the CIM presented in Szabó and Bubuŝka (1991). A more detailed explanation, mainly about implementation aspects, can be found in Pereira (2004).

Consider an integration path Γ_ρ as a circular arc of radius ρ centered in the crack tip (see Fig. 1). Assuming ρ sufficiently close to the tip, the elasticity exact solution for the displacement field can be written as

$$\{\mathbf{u}_{ex}\} = \begin{Bmatrix} u \\ v \end{Bmatrix} = \sum_{i=1}^{\infty} \frac{A_i^{(1)}}{2G} r^{\lambda_i^{(1)}} \left\{\Psi_i^{(1)}(\theta)\right\} + \sum_{i=1}^{\infty} \frac{A_i^{(2)}}{2G} r^{\lambda_i^{(2)}} \left\{\Psi_i^{(2)}(\theta)\right\}, \tag{9}$$

where G is the shear modulus, $A_i^{(1)}$ and $A_i^{(2)}$ are the so-called generalized SIFs, $\lambda_i^{(1)}$ and $\lambda_i^{(2)}$ are the eigenvalues of the solution and $\left\{\Psi_i^{(1)}(\theta)\right\}$ and $\left\{\Psi_i^{(2)}(\theta)\right\}$ are the eigenfunctions of the solution. These eigenvalues and eigenfunctions can be consulted in Szabó and Babuŝka (1991). For closed crack (α = 360°), for example, $\lambda_i^{(1)} = -0.50$ and $\lambda_i^{(2)} = -0.50$. It is also noted that the superscripts (1) and (2) indicate Mode I and Mode II, respectively.

The respective traction vector for Eq. (9) can be written as

$$\left\{\mathbf{T}^{(\mathbf{u}_{ex})}\right\} = \begin{Bmatrix} T_x \\ T_y \end{Bmatrix} = \sum_{i=1}^{\infty} A_i^{(1)} \lambda_i^{(1)} \rho^{\lambda_i^{(1)}-1} \left\{\Upsilon_i^{(1)}(\theta)\right\} + \sum_{i=1}^{\infty} A_i^{(2)} \lambda_i^{(2)} \rho^{\lambda_i^{(2)}-1} \left\{\Upsilon_i^{(2)}(\theta)\right\}, \tag{10}$$

where $\left\{\Upsilon_i^{(1)}(\theta)\right\}$ and $\left\{\Upsilon_i^{(2)}(\theta)\right\}$ can be found in Szabó and Babuŝka (1991).

Additionally, a displacement field for an auxiliary problem, also called extraction function, is defined as

$$\left\{\mathbf{w}_{-j}^{(m)}\right\} = \frac{1}{c_j^{(m)}(\alpha)} \cdot \frac{1}{2G} r^{\lambda_{-j}^{(m)}} \left\{\Psi_{-j}^{(m)}\right\} \tag{11}$$

$\left\{\mathbf{w}_{-j}^{(m)}\right\}$ is composed by negative eigenvalues ($\lambda_{-j}^{(m)} = -\lambda_j^{(m)}$) and the constants $c_j^{(m)}(\alpha)$ correspond to the extraction functions coefficients, whose values can be found in Pereira (2004).

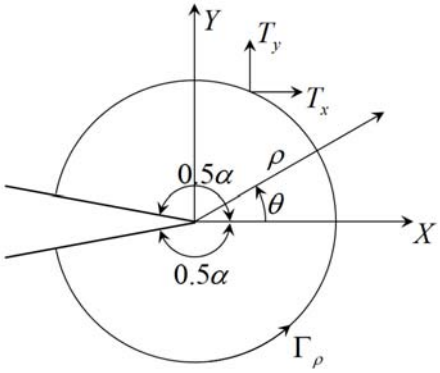

Figure 1 – Circular integration path (Γ_ρ) near to the crack tip. (adapted from Pereira (2004))

On the boundary Γ_ρ the traction vector, refers to the extraction function $\left\{\mathbf{w}_{-j}^{(m)}\right\}$, is:

$$\left\{\mathbf{T}_{-j}^{\left(\mathbf{w}_{-j}^{(m)}\right)}\right\} = \frac{1}{c_j^{(m)}(\alpha)} \cdot \lambda_{-j}^{(m)} \cdot \rho^{\lambda_{-j}^{(m)}-1} \left\{Y_{-j}^{(m)}\right\}. \tag{12}$$

Now, considering the independence of the integration path is possible to establish that:

$$A_j^{(m)} = \int_{\Gamma^*} \left\{\mathbf{w}_{-j}^{(m)}\right\}^T \left\{\mathbf{T}^{(\mathbf{u}_{ex})}\right\} ds - \int_{\Gamma^*} \left\{\mathbf{u}_{ex}\right\}^T \left\{\mathbf{T}_{-j}^{\left(\mathbf{w}_{-j}^{(m)}\right)}\right\} ds \tag{13}$$

for arbitrary Γ^*. A priori the values of $\{\mathbf{u}_{ex}\}$ and $\left\{\mathbf{T}^{(\mathbf{u}_{ex})}\right\}$ are unknown, so is convenient replace them by numerical approximations. In this work, these approximations are provided by the GFEM and by the SGFEM. Furthermore, it is hereby also proposed replace $\left\{\mathbf{T}^{(\mathbf{u}_{ex})}\right\}$ by the $\left\{\mathbf{T}^{(\boldsymbol{\sigma}_{rec})}\right\}$, whose differential is the use of the recovered stresses.

The last step is compute the SIFs considering the relations below

$$K_I = \sqrt{2\pi} A_1^{(1)}; K_{II} = \sqrt{2\pi} A_1^{(2)} \tag{14}$$

RECOVERED STRESSES

Based in Lins et al. (2015), the recovered stresses $\boldsymbol{\sigma}^*$ are given by

$$\boldsymbol{\sigma}^* = \begin{Bmatrix} \sigma_{xx}^* \\ \sigma_{yy}^* \\ \tau_{xy}^* \end{Bmatrix} = \sum_{i=1}^{n} \varphi_i \begin{pmatrix} a_{xx,i}^* \\ a_{yy,i}^* \\ a_{xy,i}^* \end{pmatrix} + \sum_{j=1}^{nh} \varphi_j \begin{pmatrix} \sum_{q=1}^{3} H_{L,q} b_{xx,j}^* \\ \sum_{q=1}^{3} H_{L,q} b_{yy,j}^* \\ \sum_{q=1}^{3} H_{L,q} b_{xy,j}^* \end{pmatrix} + \sum_{k=1}^{nb} \varphi_k \begin{pmatrix} \sum_{m=1}^{2} g_{xx,m} c_{xx,km}^* \\ \sum_{m=1}^{2} g_{yy,m} c_{yy,km}^* \\ \sum_{m=1}^{2} g_{xy,m} c_{xy,km}^* \end{pmatrix} \tag{15}$$

In Eq. (15), n denotes the total number of nodes, nh indicates the number of nodes enriched by linear Heaviside functions and nb represents the number of nodes enriched by OD functions. The functions $g_{pq,m}$ are related to the pure mode I and II stress components and can be found in Lins et al. (2015). The values $a_{pq,i}$, $b_{pq,j}$ and $c_{pq,k}$ can be interpreted as nodal parameters associated to the recovered stresses and can be computed from the minimization of the following functional (see Zienkiewicz and Zhu (1987)):

$$\Pi = \int_{\Omega} \left(\boldsymbol{\sigma}^* - \hat{\boldsymbol{\sigma}}\right)^T \left(\boldsymbol{\sigma}^* - \hat{\boldsymbol{\sigma}}\right) d\Omega, \tag{16}$$

where $\hat{\sigma}$ is the stress field computed directly from the GFEM or SGFEM solution and Ω is the analysis domain. This minimization is reinterpreted as a locally weighted L^2 projection in Lins et al. (2019) with basis on work of Schweitzer

(2013). In this strategy hereby adopted, the nodal parameters associated to the recovered stresses are obtained from the following linear system of equations for each stress component $\boldsymbol{\sigma}_d^*$, d = *xx*, *yy*, *xy* = 1, 2, 3:

$$\widetilde{\mathbf{A}}^d \widetilde{\mathbf{a}}^d = \mathbf{f}^d, \tag{17}$$

where vector $\tilde{\mathbf{a}}^d$ gathers the coefficients $a_{pq,i}$, $b_{pq,j}$ and $c_{pq,k}$ presented in Eq. (15). The entries of matrix $\tilde{\mathbf{A}}^d$ and vector $\mathbf{f}^d$ are respectively given by

$$\widetilde{A}^d_{(\alpha,i),(\beta,j)} = \begin{cases} 0 & \text{if } \alpha \neq \beta \\ \int_\Omega \left(g^d_{\alpha i} g^d_{\beta j} \right) \varphi_\beta d\Omega & \text{if } \alpha = \beta \end{cases} \tag{18}$$

$$f^d_{(\beta,j)} = \int_\Omega \hat{\sigma}^d \varphi_\beta g^d_{\beta j} d\Omega, \tag{19}$$

with α and β associated to nodes assuming values equal to 1, 2, …, n and i and j associated to the functions $g_{pq,m}$ assuming values equal to 0, 1, 2.

Matrix $\tilde{\mathbf{A}}^d$ is symmetric, positive-definite and block diagonal leading to a computationally efficient and robust strategy for computing the recovered stress tensor. More details about this strategy, including a series of results, can be found in Lins et al. (2019).

NUMERICAL EXAMPLES

In this section, the employment of the recovered stresses to improve the CIM performance is evaluated considering two benchmark problems of the fracture mechanics. For both problems, the accuracy and the path independence are investigated by means of 50 circular integration paths localized between two limits (10% and 90%) related to the enriched zone size (see Fig. 2). Furthermore, the relative error in the SIFs computation is computed as

$$e_K = \frac{|K - K_{REF}|}{K_{REF}} \cdot 100\% \tag{20}$$

In all computations, 16 Gaussian points are used in the evaluation of the contour integrals. Finally, for the implementation and extraction of results, the GFEM/SGFEM dedicated object-oriented programming toolkit named SCIEnCE (see Piedade Neto (2013)) was used.

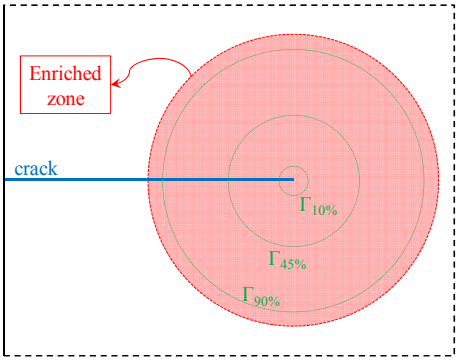

Figure 2 – Localization of the circular integration paths used to evaluate the CIM performance

Shear edge crack

In this example, the panel with a shear edge crack depicted in Fig. 3a is analyzed. According to Yau at al. (1980), the reference mixed mode SIFs for this problem are: $K_{\text{I,REF}}$ = 34.00 and $K_{\text{II,REF}}$ = 4.55. The geometry, the adopted boundary conditions and the considered physical parameters are also indicated in Fig. 3a. In addition, plane strain conditions and dimensionless measurements are assumed.

Four uniform and structured meshes composed of bilinear quadrilateral elements are adopted. They present the following grid sizes: 11x25, 25x47, 47x95 and 95x191. The 11x25 mesh with its enriched nodes is shown in Fig. 3b. For all meshes, geometric singular enrichments (OD functions) are applied to the nodes belonging to a circular region (radius = 1.75) centralized at the crack tip. Additionally, singular enrichments are also applied to other nodes belonging to elements crossed by crack (see Fig. 3b).

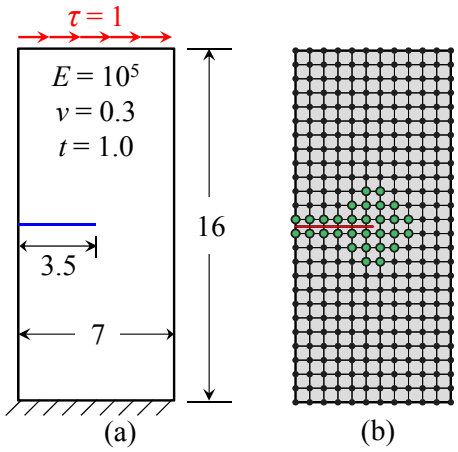

Figure 3 – Shear edge crack: (a) geometry, boundary conditions and physical parameters; (b) Mesh with grid size 11x25 and its enriched nodes highlighted in green.

Accuracy of the SIFs

Table 1 presents the mean relative error of SIFs computations considering all integration paths. The SIFs are computed by the CIM considering or not the recovered stresses. In general, the results indicate that the accuracy is improved when the recovered stresses are considered, mainly for GFEM results and mode II. For mesh 2, for example, the recovered stresses more than duplicate the accuracy of the GFEM for both modes. Furthermore, it is interesting to realize that the benefits introduced by recovered stresses end being less meaningful when the refinement increases considerably (Mesh 4).

Table 1 – Mean relative error (%) of SIFs computations considering all integration paths.

Mesh ID	N° DOF	Mode I (K_I)				Mode II (K_{II})			
		Raw Stresses		Rec. Stresses		Raw Stresses		Rec. Stresses	
		GFEM	SGFEM	GFEM	SGFEM	GFEM	SGFEM	GFEM	SGFEM
1	744	2.4437	1.1611	3.3063	1.8461	1.3521	1.0779	1.3772	1.0334
2	2952	1.2441	0.2319	0.5340	0.2852	0.8998	0.4570	0.4087	0.3516
3	10848	0.4529	0.0772	0.0535	0.0405	0.4041	0.3256	0.3062	0.2926
4	43344	0.1661	0.1070	0.0836	0.1045	0.3135	0.2980	0.2957	0.2922

Path independence in SIFs computation

Table 2 indicates the standard deviation in SIFs values considering all integration paths. Clearly, the path independence is not guaranteed when the raw stresses are chosen as input in the CIM, even in the SGFEM that presents better results. On the other hand, when the recovered stresses are chosen, the standard deviation is much lower for all cases. This effect can be seen in more details with the help of Fig. 4, where the K_{II} value is plotted along of different integrations paths for mesh 2 considering recovered stresses and raw stresses provided by the GFEM.

Table 2 – Standard deviation in SIFs values considering all integration paths.

Mesh ID	N° DOF	Mode I (K_I)				Mode II (K_{II})			
		Raw Stresses		Rec. Stresses		Raw Stresses		Rec. Stresses	
		GFEM	SGFEM	GFEM	SGFEM	GFEM	SGFEM	GFEM	SGFEM
1	744	0.9005	0.2264	0.5421	0.1988	0.0768	0.0558	0.0365	0.0243
2	2952	0.5159	0.0821	0.0984	0.0657	0.0460	0.0168	0.0061	0.0080
3	10848	0.1879	0.0268	0.0222	0.0087	0.0181	0.0057	0.0023	0.0032
4	43344	0.0729	0.0104	0.0028	0.0022	0.0094	0.0019	0.0006	0.0009

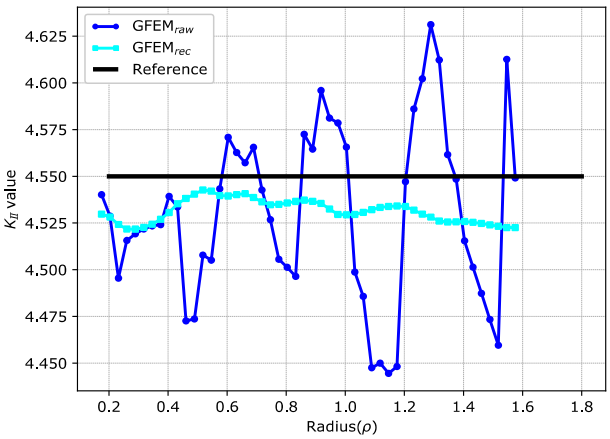

Figure 4 – Variation of K_{II} value along of integration paths for mesh 2

Inclined center crack

The inclined center crack analyzed in this example is depicted in Fig. 5a. The reference SIFs for this problem are gathered in Tab. 3 and were extracted from Murakami (1987). Neumann boundary conditions (self-equilibrated external loading), the geometry and the adopted physical parameters are also indicated in Fig. 5a. Once again, plane strain conditions and dimensionless measurements are assumed.

Four structured meshes composed of linear triangular elements are adopted for each inclination α. They present the following grid sizes: 11x19, 19x41, 41x79 and 79x161. The 11x19 mesh with its enriched nodes considering an inclination $\alpha = 45°$ is shown in Fig. 5b. For all meshes, geometric singular enrichments (OD functions) are applied to the nodes belonging to a circular region (radius = 2.00) centralized at the crack tips. Moreover, linear discontinuous enrichments (linear Heaviside) are applied to other nodes belonging to elements crossed by crack (see Fig. 5b).

Table 3 – Reference SIFs for inclined center crack

α (degrees)	K_I	K_{II}
15	3.7402	0.8366
30	3.0209	1.4736
45	2.0296	1.7419
60	1.0229	1.5417

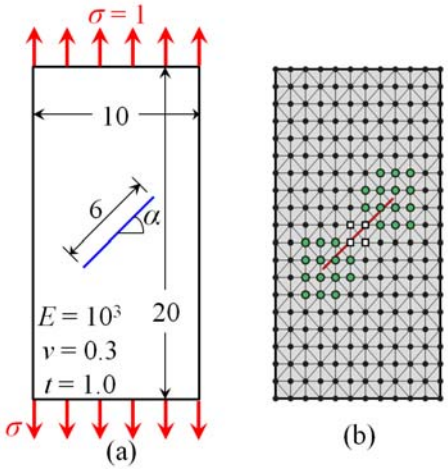

Figure 5 – Inclined center crack: (a) geometry, boundary conditions and physical parameters; (b) Mesh with grid size 11x19 and $\alpha = 45°$ and its enriched nodes highlighted in green (singular enrichments) or white (discontinuous enrichment).

Accuracy of the SIFs

Table 4 shows the mean relative error of SIFs computations considering all integration paths for all meshes. Each presented value corresponds to a simple mean of the four obtained values associated to analyzed meshes in each inclination α. Once again, the SIFs are computed by the CIM considering or not the recovered stresses. On average,

specifically in mode I, the recovered stresses are responsible to increase the accuracy in approximately 39% for results provided by the GFEM and in approximately 21% for SGFEM case. For mode II, these numbers change a little. The improvement in the GFEM results is about 42%, whereas in SGFEM case is about 22%.

Table 4 – Mean relative error (%) of SIFs computations considering all integration paths for all meshes. The presented value is a simple mean of values obtained for the four meshes analyzed in each inclination.

α	Mode I (K_I)				Mode II (K_{II})			
	Raw Stresses		Rec. Stresses		Raw Stresses		Rec. Stresses	
	GFEM	SGFEM	GFEM	SGFEM	GFEM	SGFEM	GFEM	SGFEM
15°	2.2706	1.1255	1.3573	1.1255	4.1899	2.4963	0.8290	0.9858
30°	2.1049	1.0500	1.4138	1.0786	2.3018	1.9597	1.6414	1.8075
45°	2.4389	1.7084	1.5380	1.2276	2.0782	1.5010	1.9147	1.6894
60°	2.8743	2.0724	1.5690	1.2766	2.3729	1.6626	1.9375	1.4693

Path independence in SIFs computation

Table 5 presents the standard deviation in SIFs values considering all integration paths for all meshes. It is necessary to clarify again that each presented value, in fact, corresponds to a simple mean of four values obtained considering the four evaluated meshes in each inclination α. Undoubtedly, the employment of the recovered stresses in the CIM reduces the standard deviation becoming this technique more close to the path independence. For instance, in the mode I, the standard deviation is reduced on average in approximately 59% considering results provided by the GFEM and in approximately 46% for the SGFEM results. For mode II, these numbers change for 42% and 30%, respectively. Figure 6 depicted below corroborate these observations, presenting the variation of the K_{II} values computed for mesh 2 (grid size 19x41) and a crack inclination of 15°.

Table 5 – Standard deviation in SIFs values considering all integration paths for all meshes. The presented standard deviation is a simple mean of values obtained for the four meshes analyzed in each inclination.

α	Mode I (K_I)				Mode II (K_{II})			
	Raw Stresses		Rec. Stresses		Raw Stresses		Rec. Stresses	
	GFEM	SGFEM	GFEM	SGFEM	GFEM	SGFEM	GFEM	SGFEM
15°	0.091	0.040	0.041	0.028	0.0421	0.0254	0.0085	0.0074
30°	0.068	0.031	0.029	0.014	0.0352	0.0337	0.0249	0.0301
45°	0.053	0.041	0.021	0.019	0.0420	0.0259	0.0339	0.0229
60°	0.032	0.019	0.009	0.010	0.0362	0.0233	0.0225	0.0159

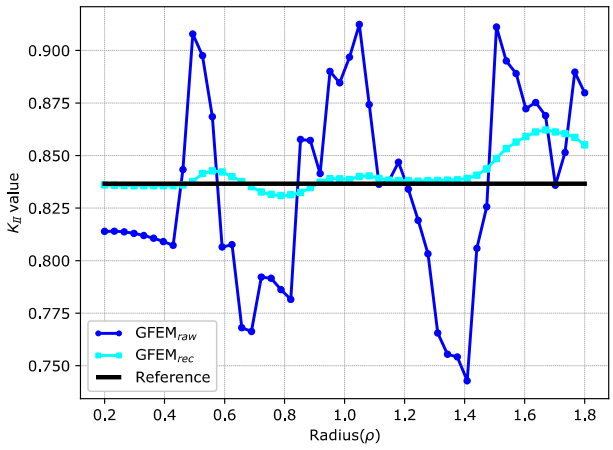

Figure 6 – Variation of K_{II} value along of integration paths for mesh 2 and a crack inclination α of 15°

FINAL CONSIDERATIONS

This work presented a new application for the recovered stresses, commonly used for constructing of error estimators. Herein, the recovered stresses were utilized replacing the raw stresses provided by the GFEM and the SGFEM in the CIM. The main objective of this new application is to improve the SIFs computation in terms of accuracy and independence of the integration paths. The main findings of this work are summarized in the following:

Accuracy of the SIFs: in general, there is an improvement in accuracy of SIF's computed by the CIM using the recovered stresses, mainly for the GFEM results. However, this improvement could not be seen for coarse meshes, probably in consequence of the high imprecision of the displacement fields directly provided by the GFEM and the SGFEM.

Path independence in SIFs computation: the employment of the recovered stresses allows to decrease in accentuated way the variation of the SIF's along of the integration paths both for the GFEM and for the SGFEM.

Concerning possible future works, it would be natural to investigate in what way the recovered stresses could modify the performance of other extraction methods based on energy release rate.

ACKNOWLEDGMENTS

The authors would like to gratefully acknowledge São Paulo Research Foundation (FAPESP) for the financial support for this research project (2020/08308-8) and CNPq, grant number 311972/2020-9.

REFERENCES

Anderson, T.L., 2005, "Fracture Mechanics – Fundamentals and Applications", 3rd Edition, Ed. Taylor and Francis Group, USA, 621p.

Babuška, I. and Banerjee, U., 2012, "Stable Generalized Finite Element Method (SGFEM)". Comput Methods Appl Mech Eng, Vol. 201, pp. 91-111.

Belytschko, T., Gracie, R. and Ventura, G., 2009, "A review of extended/generalized finite element methods for material modeling". Model Simul Mater Sci Eng, 17:043001.

Duarte, C.A., Babuška, I. and Oden, J.T., 2000, "Generalized Finite Element Methods for Three-Dimensional Structural Mechanics Problems", Computer & Structures, Vol. 77, pp. 215-232.

Fries, T-P and Belytschko, T., 2010, "The generalized/extended finite element method: an overview of the method and its applications". Int J Numer Methods Eng, Vol. 84, pp. 253-304.

Gupta, V., Duarte, C. A., Babuška, I. and Banerjee, U., 2013, "A stable and optimally convergent generalized FEM (SGFEM) for linear elastic fracture mechanics", Comput Methods Appl Mech Eng, Vol 266, pp. 23-39.

Lins, R.M., Ferreira, M.D.C., Proença, S.P.B. and Duarte, C.A., 2015, "An a-posteriori error estimator for linear elastic fracture mechanics using the stable generalized/extended finite element method", Computational Mechanics, Vol. 56, pp. 947-965.

Lins, R.M., Proença, S.P.B. and Duarte, C.A., 2019, "Efficient and accurate stress recovery procedure and a posteriori error estimator for the stable generalized/extended finite element method", Int J Numer Methods Eng, Vol. 119, pp. 1-28.

Marukami, Y., 1987, "Stress Intensity Factors Handbook", Pergamon Press, Oxford.

Oden, J.T. and Duarte, C.A., 1997, "Clouds, cracks and FEM's", In: Recent Developments in Computational and Applied Mechanics, Reddy DB, ed. Barcelona, Spain: International Center for Numerical Methods in Engineering, CIMNE, pp. 302-321.

Pereira, J.P. and Duarte, C.A., 2005, "Extraction of stress intensity factors from generalized finite element solutions", Eng Anal Boundary Elem, Vol. 29, pp. 397–413

Pereira, J.P.A., 2004, "Extração de fatores de intensidade de tensão utilizando a solução do método dos elementos finitos generalizados", MS Thesis, Universidade de São Paulo, São Carlos, Brazil.

Piedade Neto, D., Ferreira, M.D.C. and Proença, S.P.B., 2013, "An object-oriented class design for the generalized finite element method programming", Latin Am J Solids Struct, Vol. 10, pp. 1267-1291.

Prange, C., Loehnert, S. and Wriggers, P., 2012, "Error estimation for crack simulations using the XFEM", Int J Numer Methods Eng, Vol. 91, pp. 1459-1474

Rice, J.M., 1968, "A Path Independent Integral and the Approximate Analysis of Strain Concentration by Notches and Cracks", Journal of Applied Mechanics, Vol. 35, pp. 379-386.

Schweitzer, M.A., 2013, "Variational mass lumping in the partition of unity", SIAM J Sci Comput, Vol. 35, pp. 1073-1097.

Szabó, B. and Babuška, I., 1991, "Finite element analysis", Ed. Wiley, USA, 384p.

Yau, J., Wang, S. and Corten H., 1980, "A mixed-mode crack analysis of isotropic solids using conservation laws of elasticity", Journal of Applied Mechanics, Vol. 47, pp. 335-341.

Zienkiewicz, O.C. and Zhu, J.Z., 1987, "A simple error estimator and adaptive procedure for practical engineering analysis", Int J Numer Methods Eng, Vol. 24, pp. 337-357.

RESPONSIBILITY NOTICE

The author(s) is (are) the only party(ies) responsible for the printed material included in this paper.